# Mechanisms of Solvent Evaporation Encapsulation Processes: Prediction of Solvent Evaporation Rate

JUAN WANG AND STEVEN P. SCHWENDEMAN*

Contribution from *Division of Pharmaceutics, College of Pharmacy, The Ohio State University, 500 West 12th Avenue, Columbus, Ohio 43210.*

Received April 17, 1998. Final revised manuscript received September 15, 1998.
Accepted for publication July 15, 1999.

**Abstract** □ The mechanism of organic solvent evaporation during microencapsulation and its role during microsphere hardening has been investigated. Evaporation and encapsulation studies were carried out in a jacketed beaker, filled with aqueous hardening solution, which was maintained at constant temperature and constant stirring rate in the turbulent regime. Evaporation of dissolved methylene chloride (MC), ethyl acetate (EA), and acetonitrile (ACN) was examined by the decline in organic solvent concentration in the hardening bath, which was monitored by gas chromatography. The evaporation from the bath followed first-order kinetics under dilute conditions (e.g., MC < 3 mg/mL), yielding an overall permeability coefficient, *P*. The value of *P* was theoretically related to the Kolmogorov length-scale of turbulence under conditions that favor liquid-side transport control. According to theory, factors that favored liquid-phase control (as opposed to gas-phase control) were those that favored a high Henry's law constant [i.e., elevated temperature near the normal boiling point (bp) of the organic solvent] and properties of the dissolved organic solvent (i.e., low normal bp and low aqueous solubility). These theoretical hypotheses were confirmed by (1) correlating the experimentally determined *P* with process variables raised to the appropriate power according to theory, $r^2 = 0.95$ (i.e., $P \propto$ rotational speed, $\omega^{3/4}$, impeller diameter, $d^{5/4}$, volume of hardening bath, $V^{-1/4}$, and the product of kinematic viscosity and diffusion coefficient, $\nu^{-5/12}D^{2/3}$), and (2) illustrating that at constant temperature, the tendency of the evaporation system to obey liquid-side transport control follows the same order of increasing Henry's law constant (i.e., MC > EA > ACN). To establish the relationship of evaporation with microsphere hardening, the decline in MC concentration was determined in both the continuous and dispersed polymer phases during microencapsulation. By applying a mass balance with respect to MC in the hardening bath, the cumulative hardening profile of the microspheres was accurately predicted from the interpolating functions of the kinetics of MC loss from the bath with and without polymer added. These results have potential use for microsphere formulation, design of encapsulation apparatus, and scale up of microsphere production.

## Introduction

The solvent evaporation encapsulation method has been widely used for preparation of microspheres for the controlled release of drugs. During encapsulation, a single oil-in-water (o/w) emulsion is commonly used for un-ionized and lipophilic drugs, and a double w/o/w emulsion is often used for the encapsulation of hydrophilic or ionized compounds, such as proteins and peptides.[1] Despite the widespread use of this technique, encapsulation methodologies are still largely based on trial and error. More quantitative theory and experiments are required to improve our understanding of how the encapsulation conditions affect the final particle characteristics. Such studies also may help to reduce batch-to-batch variation, organic solvent residual content, and scale up difficulties.

The physical chemical events that take place between emulsion formation to eventual microsphere hardening can be separated into several components; such as diffusion of the organic solvent from the embryonic particles into the aqueous hardening bath, evaporation of the solvent, polymer phase separation at the microsphere surface, particle coalescence, and drug loss into the hardening bath. Among these coupled events, the rate of solvent evaporation will directly influence the organic solvent level in the hardening bath, which in turn will influence the chemical potential gradient of the same species across the particle hardening surface, and consequently, the solvent removal rate. It has been shown that the solvent removal rate can have significant effect on the microsphere properties.[1−5] Therefore, the evaporation rate kinetics was selected as a logical place to begin quantitative evaluation of these coupled physical chemical events during microsphere preparation.

The objectives of this paper were (1) to devise a theory to relate process conditions to organic solvent evaporation rate from a stirred aqueous hardening bath, (2) to test such a theory experimentally by measuring solvent evaporation kinetics, and (3) to use the theoretical model to predict the kinetics of microsphere hardening during encapsulation by simultaneously monitoring the kinetics of organic solvent levels in the continuous phase of the hardening bath.

## Theoretical Section

**Definition of Permeability Coefficients**—Consider a system consisting of a stirred jacketed beaker filled with an aqueous hardening bath maintained at constant temperature, as shown in Figure 1A. An overhead mixer rotates an impeller of type shown in Figure 1B at constant rotational speed sufficient to induce turbulent flow [e.g., the impeller Reynolds number (*Re*) >1000 for the system described in Figure 1].[6] *Re* is defined as

$$Re \equiv \frac{\omega d^2}{\nu} \tag{1}$$

where $\omega$, $d$, and $\nu$ are the rotational speed, impeller diameter, and fluid kinematic viscosity, respectively.

When a volatile organic solvent is introduced in the aqueous hardening bath below its aqueous solubility, the solvent dissolves and begins to evaporate. The solvent either is added directly or accumulates during hardening of the polymer microspheres. Let an overall (or total) permeability coefficient (equivalent to overall mass transfer

* To whom correspondence should be addressed. Telephone: (614)-688-3797. Fax (614)292-7766. E-mail: schwende@dendrite.pharmacy.ohio-state.edu.


10.1021/js980169z CCC: $18.00
*Published on Web 09/03/1999*

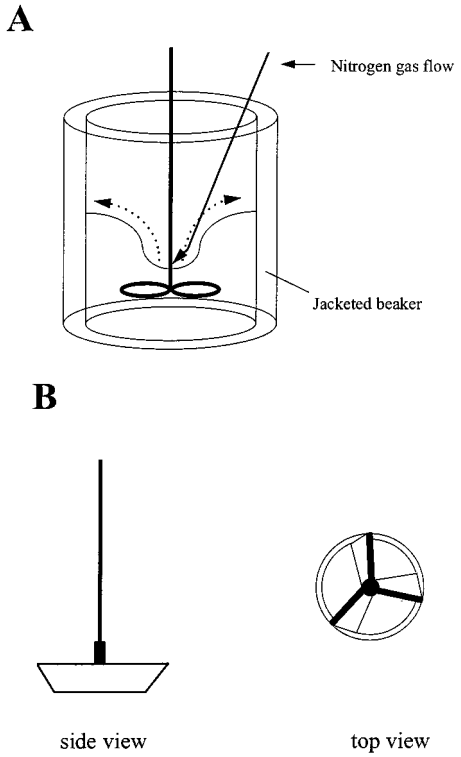


**Figure 1**—Stirring apparatus used to assess evaporation from the hardening bath. (A) A jacketed beaker was maintained under constant rotational speed and temperature. In some cases, a light flow of $N_2$ gas was delivered across the air/water interface to disrupt the gas-phase boundary layer. (B) Side and top views of the turbine impeller used to mix the bath.

coefficient) at the air/liquid interface, $P$, be defined in the usual way from the quotient of mass flux of the evaporating organic solvent, $j_s$, and the difference in bulk concentration in the bath (continuous phase), $C$, and some point in space above the bath where the concentration becomes zero; that is

$$P \equiv \frac{j_s}{\Delta C} = \frac{j_s}{C - 0} = \frac{j_s}{C} \tag{2}$$

The $P$ may be separated into contributions of the liquid and gas sides according to eq 3[7]

$$\frac{1}{P} = \frac{1}{P_L} + \frac{1}{H \cdot P_G} \tag{3}$$

where $P_L$ and $P_G$ are the liquid-side and gas-side permeability coefficients, respectively, and $H$ is Henry's law constant.

**Organic Solvent Mass Balance in the Hardening Bath**—A mass balance with respect to the organic solvent in the continuous phase during hardening of the microspheres yields

$$V\frac{dC}{dt} = R_H - R_E = R_H - PAC \tag{4}$$

where $V$, $R_H$, $R_E$, $A$, and $t$ are the volume of the fluid, overall rate of organic solvent removal from microspheres (or hardening rate), rate of solvent evaporation, air/water surface area, and time, respectively.

To determine $P$, let $R_H = 0$ by addition of organic solvent directly (i.e., no microspheres) and the concentration in the solvent bath is monitored. $P$ has been reported to be independent of $C$,[4,7,8] which results in first-order evaporation kinetics. In this case, integration of eq 4 gives

$$C = C_0\, e^{-P\frac{A}{V}t} \tag{5}$$

where $C_0$ is the initial organic solvent concentration in the bath. During encapsulation, $R_H > 0$ and integration gives an expression for cumulative mass removed from microspheres, $M_H$, as follows:

$$M_H \equiv \int_0^t R_H\, dt = V[C(t) - C_0] + A\int_0^t PC\, dt \tag{6}$$

Hence, the cumulative solvent removed may be related to the permeability coefficient and the concentration−time profile in the continuous phase during encapsulation.

**Calculation of the Kolmogorov Length-Scale**—The size of the characteristic eddy, or Kolmogorov length, $\delta_K$, induced by turbulence originating from the energy input from the impeller, is[9]

$$\delta_K = \left(\frac{\nu^3}{\epsilon}\right)^{1/4} \tag{7}$$

where $\epsilon$ is the energy dissipation rate per unit mass of fluid. The Kolmogorov length can be described as the length scale of the smallest eddy at which inertial forces equal viscous forces. In turbulent fluids, large eddies become unstable and cascade into smaller eddies without energy loss until $\delta_K$ is reached. At $\delta_K$ eddies disappear losing their kinetic energy to thermal energy.

To calculate $\delta_K$, $\epsilon$ must be determined. For isotropic turbulence, $\epsilon$ is equivalent to the rate of energy loss from the impeller to the fluid, $\dot{Q}$, divided by the mass of fluid ($\rho V$). $\dot{Q}$ is given as[10]

$$\dot{Q} = N_p \rho \omega^3 d^5 \tag{8}$$

where $\rho$ is the density and $N_p$ is the dimensionless power number, which is dependent on the impeller type and thickness, as well as the presence or absence of baffles in the tank.

Thus, in a hardening tank containing a fluid volume, $V$, by combining eqs 7 and 8, $\delta_K$ becomes

$$\delta_K = \left[\frac{\nu^3}{(N_p \rho \omega^3 d^5/\rho V)}\right]^{1/4} = \left[\frac{Vd}{N_p\left(\frac{\omega^3 d^6}{\nu^3}\right)}\right]^{1/4} = \frac{(Vd)^{1/4}}{N_p{}^{1/4} Re^{3/4}} \tag{9}$$

**Estimating the Liquid-Side Boundary Layer Thickness, $\delta_D$**—The movement of the fluid near an air/liquid interface is somewhat more controversial than near a solid/liquid interface. Near a solid/liquid interface, the turbulence is damped within a viscous sublayer, $\delta_V$, over which the bulk mean velocity is dissipated with the square of position toward the interface.[8] At the interface, the fluid velocity becomes zero in all directions. Near an air/liquid interface, only the velocity component normal to the surface is zero. At a 'clean' interface (i.e., a surface free of contaminants), the vertical mean velocity is dissipated linearly with position toward the interface, and the boundary layer thickness, $\delta_D$ ($=D/P_L$), is given as[8]

$$\delta_D \propto \delta_V Re^{*-1/2} Sc^{-1/2} \tag{10}$$

where $Re^*$ is the local Reynolds number, $u_e \cdot \delta_e/\nu$, of approaching eddies ($u_e$ and $\delta_e$ are velocity and length scale of the eddy, respectively) to the interface, and $Sc$ is the

Schmidt no. ($\nu/D$), where $D$ is the diffusion coefficient of the volatile species evaporating at the air/liquid interface.

Most surfaces, however, contain contaminants, especially in small-scale laboratory and industrial flows.[8] In this so-called 'dirty' interface category, surface-active substances (e.g., organic solvent molecules and surfactant molecules in the case of encapsulation by solvent evaporation) are present in excess at the surface. The mean vertical velocity component is then dissipated with the square of position (like the solid/gas interface case) and

$$\delta_D \propto \delta_e \cdot Sc^{-1/3} \tag{11}$$

If the characteristic length, $\delta_e$, is assumed to be proportional to the Kolmogorov length-scale, $\delta_K$, then

$$\delta_D \propto \delta_K \cdot Sc^{-1/3} \tag{12}$$

Finally, by assuming a constant impeller type and thickness, and turbulent flow conditions, $N_p$ becomes nearly constant[10] and $\delta_D$ may be related to system variables as follows:

$$\delta_D \propto \left(\frac{Vd}{Re^3}\right)^{1/4} Sc^{-1/3} \tag{13}$$

This result also may be given in nondimensional form. The Sherwood number, $Sh$, is equivalent to $Pd/D$. Under liquid-side transport control according to the film theory,[7] $P = P_L = D/\delta_D$ and

$$Sh = \frac{d}{\delta_D} \propto Ko \cdot Sc^{1/3} \tag{14}$$

$Ko$ is introduced as the corrected Kolmogorov number as follows:

$$Ko = \left(Re\frac{d}{\sqrt[3]{V}}\right)^{3/4} \tag{15}$$

which is defined as the ratio of the impeller diameter to the Kolmogorov length corrected for $N_p^{1/4}$; that is, $Ko \equiv d/(N_p^{1/4}\delta_K)$.

The relationship in eq 14 can also be written in a manner to test the dependence on individual variables; that is

$$P \propto d^{5/4} V^{-1/4} \omega^{3/4} \nu^{-5/12} D^{2/3} \tag{16}$$

or

$$\delta_D = D/P \propto d^{-5/4} V^{1/4} \omega^{-3/4} \nu^{5/12} D^{1/3} \tag{17}$$

Finally, it is useful to note that the same relationship may be obtained from

$$Sh \propto \left[\frac{d^4(\dot{Q}/V)}{\rho\nu^3}\right]^{1/4} \cdot Sc^{1/3} \tag{18}$$

which has been reported for mass transport at the interface of bubbles or small drops dispersed in a liquid.[7]

## Materials and Methods

**Chemicals**—Methylene chloride (MC) was purchased from Fischer Scientific with gas chromatography (GC) purity of 99.9%. High-performance liquid chromatography (HPLC) grade acetonitrile (ACN), ethyl acetate (EA), and 2-propanol were also obtained from Fisher Scientific. PRA grade chloroform (suitable for pesticide residual analysis) was purchased from Sigma-Aldrich with GC purity of 99.9%. Poly(DL-lactide-*co*-glycolide) (PLGA; 50:50; intrinsic viscosity, 0.65 dL/g in hexafluoro-2-propanol (HFIP) at 30 °C; lot no. 410-27-1A) was obtained from Birmingham Polymers, Inc., and 80% hydrolyzed poly(vinyl alcohol) (PVA; average MW 9000–10 000) was purchased from Aldrich Chemical Company. Triamcinolone acetonide was obtained from Sigma Chemical Company with 99% purity. All chemicals were used as received.

**Evaporation of Organic Solvents from Aqueous Solution**—Evaporation of organic solvents from aqueous solution was carried out in a jacketed beaker (unbaffled), which was connected with a TYP FS2N water bath (HAAKE Instruments Inc., Saddle Brook, NJ) to maintain constant temperature. Dimensions of the jacketed beaker were 59 mm i.d., 90 mm o.d., and 122 mm height. An overhead stir-tester (G. K. Heller HST 20 series) was purchased from Glas-Col (Terre Haute, IN) and used to maintain a stable rotational speed (100–900 rpm) of an axially mounted turbine impeller (see Figure 1A). Turbine stirrers (45° pitch-blade and ringed, Figure 1B) all had the same thickness (1.2 cm) and were purchased from IKA-WORKS, Inc. (Wilmington, NC; catalog nos. R1311, R1312, and R1313 for stirrers with o.d.'s of 3, 5, and 7 cm, respectively). During the study, a known amount of organic solvent was dissolved in various volumes (150–1000 mL) of double distilled water or 0.3% PVA aqueous solution at a preset temperature and constant rotational speed. Samples were taken at scheduled time intervals and assayed by GC. When examining the large stirrer diameter or large bath volume, a glass cylindrical tank (top open, 166.5 mm i.d., 87.5 mm height) placed directly into the constant temperature bath was used. The constant temperature was confirmed by reading a thermometer inserted directly in the tank.

The volume replacement after each sampling was not carried out for the organic solvent evaporation studies at low temperatures. Control experiments demonstrated that the volume loss due to sampling had little influence on the determination of permeability coefficient (data not shown). However, at relatively high temperatures ($T$ > 40 °C), the volume loss due to evaporation of water became noticeable. Under such conditions, manual water replacement was completed at 10-min intervals at a rate roughly equal to the evaporation rate so that total volume of the bath was kept nearly constant.

**Organic Solvent Analysis by Gas Chromatography**—Sample analysis was performed on a Varian series 3700 GC with a 5% Carbowax 20M 80/120 Carbopack B-AW analytical column (Supelco). The GC conditions for determination of MC, EA, and ACN in aqueous samples were as follows: $N_2$ and $H_2$ carrier gas flow rate, 30 mL/min; air flow rate, 300 mL/min; column oven temperature, 100 °C; and injector and flame ionization detector temperatures, 200 °C. For organic samples where MC was extracted by chloroform, a programmed column temperature gradient with the following settings was used: initial temperature of 100 °C for 2 min, followed by a temperature gradient of 80 °C/min, then a final temperature of 200 °C for 4 min.

**Disruption of Gas-Phase Boundary Layer by Blowing $N_2$ (g) over the Gas/Liquid Interface**—The evaporation experiments with nitrogen flow were carried out under identical conditions as the typical evaporation experiments, except that compressed nitrogen gas at room temperature was blown over the liquid/gas interface from a metal ferrule at a fixed gauge pressure (~28 psig; Figure 1A). The distal part of the metal ferrule was deformed to blow directly toward the center of the stirrer shaft to avoid violent disturbance to the surface of the evaporating solution. In this configuration, the gas was presumably forced from the bottom of the vortex outward along the surface of the liquid.

**Encapsulation of Triamcinolone Acetonide by the Solvent Evaporation Method**—The solvent evaporation encapsulation process was carried out by dissolving 2 × 800 mg of PLGA 50/50 and 2 × 40 mg of triamcinolone acetonide in 2 × 4 mL of MC in two 18 × 150-mm Pyrex glass tubes. A 1% (w/w) PVA aqueous solution (4 mL) was added to each tube, and the system was mixed for 20 s at the highest speed setting on a Vortex Genie 2 (Scientific Industries Inc., Bohemia, NY). The emulsion produced in both tubes was poured into a jacketed beaker (Figure 1A) that contained 142 mL of 0.3% PVA solution (30 °C), and the resulting mixture was stirred at 600 rpm. Samples drawn at specified times were assayed for organic solvent content. After 4 h of agitation, microspheres were collected, centrifuged, washed with double distilled water three times, freeze-dried for 2 days, and stored desiccated in microcentrifuge tubes at 4 °C.

**Determination of MC Levels in Dispersed and Continuous Phases during Encapsulation**—For MC evaporation without encapsulation, 1-mL aliquots were drawn from the hardening bath at each time point and stored at 4 °C in 1.9-mL Fisherbrand glass vials with a plastic screw cap fitted with a Teflon insert until GC analysis. A 50 $\mu$L aliquot of internal standard solution was added to each sample and mixed by vortex.

For determination of MC levels during encapsulation, samples were taken at each scheduled time point, which lasted <1 min/sample. A 0.3% PVA aqueous solution (2 mL) was replenished after each sampling procedure. For determining the MC content of the aqueous continuous phase, 1.4 mL of aqueous dispersion was withdrawn with a 5-mL polypropylene syringe and filtered through a 0.22-$\mu$m hydrophilic poly(tetrafluoroethylene) (PTFE) Millex filter unit (SE2M035J5, Millipore Corp.). Triplicate 200-$\mu$L aliquots from the filtered solution were mixed with 800 $\mu$L of pure water and 50 $\mu$L of internal standard and were subjected to GC analysis. Solvent concentrations were calculated by using a standard curve constructed with a filtered 0.3% PVA solution that contained known solvent concentrations processed by the same procedure.

For determination of MC in microspheres, the amount of MC in the dispersion was subtracted from the MC in the continuous phase. To accomplish this, triplicate 0.2-mL aliquots were taken directly from the stirred aqueous dispersion and placed in glass vials containing 0.5 mL of chloroform to prevent fast evaporation of MC. The glass vials were capped immediately. Samples were later mixed by vortex for 5 s and stored overnight at 4 °C to extract MC into chloroform before the GC analysis. The calculation of concentration of MC in the sample was based on the standard curve constructed by equilibrating a series of known amounts of MC in 0.5 mL of chloroform with 0.2 mL of 0.3% PVA aqueous solution, as in the sample preparation case. An impurity in the purchased PRA grade chloroform was used as the internal standard after appropriate validation to correct for variability in injection volume. This compound was stable in chloroform and its polarity was similar to that of MC.

The MC content in the hardening polymer phase (w/w MC/PLGA ratio) during the hardening period was calculated with eq 27, which is described in the *Data Analysis* section. The MC loss during pouring was determined gravimetrically after pouring the emulsion into a tared capped bottle.

**Determination of MC Solubility in 0.3% PVA Aqueous Solution**—A 5-mL aliquot of MC was added to 10 mL of 0.3% PVA (aq) in 20-mL scintillation vials and mixed. Samples were put on a type 50800 Thermolyne shaker (Bamstead/Thermolyne Corp., Dubugue, IA) under mild agitation in a Precision Economic Incubator (Precision Scientific, Chicago, IL) set at 30 ± 0.5 °C. Samples were taken out every 8 h and vigorously agitated. After 2 days, 200-$\mu$L aliquots were removed from the aqueous layer and mixed with 800 $\mu$L of pure water and 50 $\mu$L of internal standard, and then assayed by GC. Solubility of MC at 30 °C was determined to be 22.6 ± 0.7 mg/mL (mean ± SD, $n = 6$).

**Data Analysis**—*Calculation of the Surface Area*—Surface area, $A$, used to determine $P$ was estimated manually for each stirring condition. First, a line was drawn around the outer wall of the stirred beaker, which traced the contour of the air/water surface during the evaporation experiments. After the experiment, a piece of paper was inserted vertically into the beaker and a second line was obtained by projecting the first contour line on the paper. The surface area was calculated by integrating the strips, which were generated by rotating the projected line (which had been segmentally divided) about its center axis.[11]

*Determination of Permeability Coefficient P*—Below ~3 mg/mL (for MC), the slope of ln $C$ versus $t$ line was constant, and eq 5 is thus satisfied. The value of $P$ was determined from $P = k'V/A$, where $k'$ is the least squares slope of ln $C$ versus $t$ data. The $r^2$ was invariably >0.99.

*Estimation of Diffusion Coefficient and Kinematic Viscosity in the Hardening Bath*—The diffusion coefficients for various organic solvents in the aqueous hardening bath under different temperatures were estimated by the Wilke–Chang equation:[12]

$$D = \frac{7.4 \times 10^{-8}(\Phi M_B)^{1/2} T}{\eta_B V_A^{0.6}} \tag{19}$$

where $D$ is the mutual diffusion coefficient of organic solvent at very low concentrations in the aqueous solvent (cm$^2$/s), $M_B$ is the molecular weight of water, $T$ is the temperature (K), $\eta_B$ is the viscosity of water (cp), $V_A$ is the molar volume of organic solvent at its normal boiling temperature (cm$^3$/mol), and $\Phi$ is the association factor (2.6 for water). Values of $V_A$ for EA and ACN were taken from literature,[12] whereas the $V_A$ for MC was calculated from the average of estimation methods by Schroeder and Le Bas.[12]

$$\ln \eta_B = k_1 + k_2/T + k_3 T + k_4 T^2 \tag{20}$$

where $k_1 = -0.02471$, $k_2 = 4209$, $k_3 = 0.04527$, and $k_4 = -0.00003376$.

The kinematic viscosity was determined from the ratio of $\eta_B$ with eq 20 and $\rho$, which was obtained from literature.[10]

*Prediction of Hardening Profile from Microspheres During Encapsulation*—According to eq 6, the cumulative organic solvent removed from microspheres, $M_H$, can be expressed as a function of $V$, $A$, $C$, $P$, and $t$. Because $V$, $A$, and $C$ can be determined directly during the encapsulation experiment and $P$ can be obtained from pure evaporation experiments carried out under the same conditions as during encapsulation, the hardening profile [i.e., $M_H(t)$ versus $t$] can be predicted without direct measurement.[13]

However, most encapsulation protocols result in values of $C$ in the range where $P$ is dependent on $C$. The origin of this dependence is largely determined by the contribution of the derivative of ln(activity coefficient) with respect to ln $C$.[7] The value of $P(C)$ was determined from a series of pure evaporation experiments ($C_0 \cong C_S$) under the encapsulation conditions of interest (i.e., $V = 150$ mL, $d = 3$ cm, $T = 30$ °C, and $\omega = 600$ rpm). According to eq 4, when $R_H = 0$,

$$V\frac{dC}{dt} = -P(C)\cdot AC \tag{21}$$

which may also be written as

$$P(C) = -\frac{V}{A}\frac{d \ln C}{dt} \tag{22}$$

An $n^{th}$-order polynomial interpolating function, $p_n(\ln C)$, was fit to the $t$ versus ln $C$ data obtained during evaporation. The $P(C)$ was then determined from the derivative of the $p_n(\ln C)$ with respect to ln $C$. The interpolating function is

$$t = a_n(\ln C)^n + \ldots + a_1(\ln C)^1 + a_0 = p_n(\ln C) \tag{23}$$

The derivative, d ln $C$/d$t$, may be determined from eq 23 by using the chain rule

$$\frac{d(\ln C)}{dt} = \frac{1}{na_n(\ln C)^{n-1} + \ldots + a_1} = \frac{1}{\dfrac{d[p_n(\ln C)]}{d(\ln C)}} = \frac{1}{p_n'(\ln C)} \tag{24}$$

From eqs 22 and 24, $P(C)$ becomes

$$P(C) = -\frac{V}{A}\frac{1}{p_n'(\ln C)} \tag{25}$$

Over the entire concentration range where encapsulation occurs, eq 6 may be rewritten as follows, accounting for concentration-dependent $P(C)$:

$$M_H(t) = \int_0^t R_H dt = V[C(t) - C_0] - V\int_0^t \frac{1}{p_n'(\ln C)} C dt = V\left[q_n(t) - \int_0^t \frac{q_m(t)}{p_n'[\ln q_m(t)]} dt\right] \tag{26}$$

where $C_0 = 0$, and $q_m(t)$ is an $m$th order polynomial interpolating function for $C$ versus $t$ during encapsulation. From eq 26, the hardening profile $M_H$ was determined numerically by the Runge–Kutta method[14] on a spread sheet (time step size = 0.1 min).

*Calculation of Cumulative Amount of MC Removed, $M_H$, during Encapsulation*—The MC content in the dispersed polymer phase was calculated on the basis of the difference of MC in the total aqueous dispersion and in the continuous phase, as follows:

$$C_{DP}(t)(w/w) = \frac{[C_T(t)/\Psi(t) - C(t)]V}{M_P} \quad (27)$$

where $C_T$, $M_P$, and $\Psi$, are the measured MC content in the aqueous dispersion, the overall mass of PLGA in the dispersed system, and the ratio of the volume of the continuous phase to the volume of the entire aqueous dispersion, respectively. The value of $\Psi$ ranged from 0.95 to 1.0 in the experiment and was approximated by

$$\Psi(t) \cong 1 - \frac{C_T(t) - C(t)}{C_T(0)} \quad (28)$$

where $C_T(0)$ is the initial MC content in the aqueous dispersion.

The cumulative amount of MC removed during hardening (or the cumulative hardening profile), $M_H$, was then calculated according to the following equation:

$$M_H = V[C_{DP}{}^0 - C_{DP}(t)] \quad (29)$$

where $C_{DP}{}^0$ was estimated by the starting weight ratio of the MC to the polymer just before the emulsion was formed and then corrected by the loss of MC into the air during pouring. This loss was determined to be 4.0 ± 0.6% (mean ± SD, $n$ = 5).

## Results

**Organic Solvent Evaporation Kinetics**—The kinetics of evaporation in the hardening bath was observed to be first-order under dilute conditions ($C$ < 3 mg/mL), as shown for MC evaporation in Figure 2. Also shown in the figure is that increasing either rotational speed or temperature resulted in a faster loss of solvent from the bath (i.e., an increased evaporation rate). The slope of the first-order plots of the type in Figure 2 and the determined air/water surface area (see Experimental Section) allowed the calculation of the $P$.

**Correlation of *P* with Process Variables**—To test the correlation in eq 16, four variables were varied independently during the evaporation of MC: temperature ($T$), liquid volume ($V$), rotational speed ($\omega$), and diameter of the overhead stirrer ($d$). Among these variables, $V$, $\omega$, and $d$ directly appear in the theoretical relationship for $P$ in eq 16. The $T$ influences both kinematic viscosity of water ($\nu$) and the diffusion coefficient of organic solvent in the water ($D$). The results are shown in Figure 3.

Good linearity between $P$ and process variables, which were raised to their appropriate power according to eq 16, was observed for $\omega$, $V$, and $d$ under tested conditions. The value of $\omega$ was varied from 100 to 900 rpm, that of $V$ from 150 to 1000 mL, and that of $d$ from 3 to 7 cm. The correlation between $P$ and $\nu^{-5/12}D^{2/3}$ [i.e., $f(T)$], however, was not as successful at first glance. A significant deviation from linearity was observed at 5 °C.

Because $P_{exp}$ became nonlinear with respect to the product, $\nu^{-5/12}D^{2/3}$ at the low $T$, a partial gas-phase control was postulated. According to this postulate, the plotted data from Figure 3 obtained at $T \geq 25$ °C were combined to form a master curve, yielding a proportionality constant $a$, according to eq 16. Excellent agreement was observed ($r^2$ = 0.95), as shown in Figure 4. This high correlation strongly validates eq 16 for the prediction of $P$ for MC at $T \geq 25$ °C.

**Contribution of the Gas-Phase Unstirred Layer to the Overall Mass Transport Resistance**—To understand the deviation from eq 16 by the MC data at low $T$ in Figure 3 and to understand the rate-limiting step for mass transport during organic solvent evaporation, the evaporation of two additional solvents, EA and ACN, were studied. In addition, a light flow of nitrogen gas across the air/water interface was included in the experimental procedure to disturb any unstirred layer in the gas phase. It was assumed that by blowing the $N_2$ (g) over the surface of the liquid, the unstirred layer in the gas phase would be mixed, shifting the rate-determination step (transport control step) to the liquid side. It was also assumed that the light flow of gas would have little effect on the boundary layer in the liquid phase because the $N_2$ gas flow did not have a direct impact on the gas/liquid interface; that is, the liquid surface contour was not significantly distorted.

Because $T$ appeared to play a role in the transport control of MC in Figure 3, the temperature was varied with and without $N_2$ flow during the evaporation of the three solvents. As shown in Figure 5, the flow of $N_2$ gas increased the $P$ in all cases. However, in the two experiments

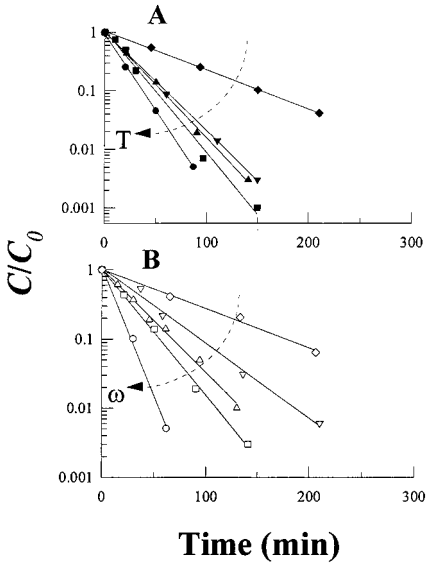


**Figure 2**—Loss of MC in the hardening bath follows first-order kinetics under dilute condtions. (A) Temperature was varied from 5 (◆), to 25 (▲), to 30 (▼), to 35 (■) and to 40 (●) °C while maintaining $\omega$, $V$, and $d$ at 600 rpm, 150 mL, and 3 cm, respectively. (B) Rotational speed was varied from 100 (◇), to 300 (▽), to 450 (△), 600 (□), and 900 (○) rpm, while maintaining $T$, $V$, and $d$ at 30 °C, 150 mL, and 3 cm, respectively.

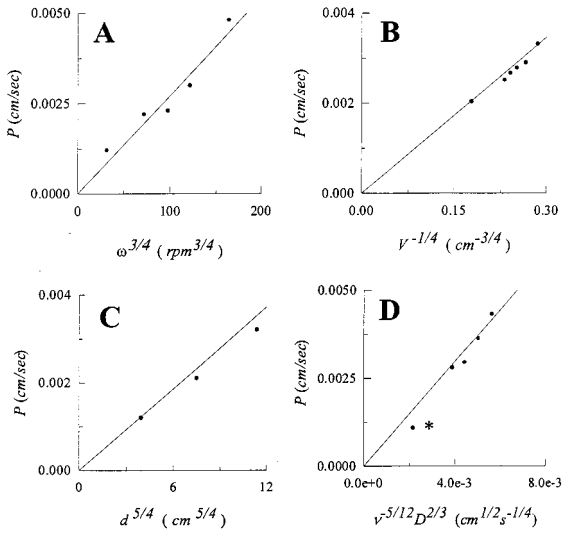


**Figure 3**—Correlation of process variables with permeability coefficient $P$. The measured $P$ was correlated with (A) $\omega^{3/4}$ at constant $T$, $V$, and $d$; (B) $V^{-1/4}$ at constant $\omega$, $T$, and $d$; (C) $d^{5/4}$ at constant $\omega$, $T$, and $V$; and (D) $\nu^{-5/12}D^{2/3}$ (variation of $T$) at constant $\omega$, $\nu$, and $d$. The theoretical lines were produced from the master curve in Figure 4. Constant conditions were $T$ = 30 °C (303 K), $\omega$ = 600 rpm, $V$ = 150 mL, and $d$ = 3 cm. * The evaporation mechanism at the lowest temperature ($T$ = 278 K) was governed by both the gas and liquid phases (see Figure 5).

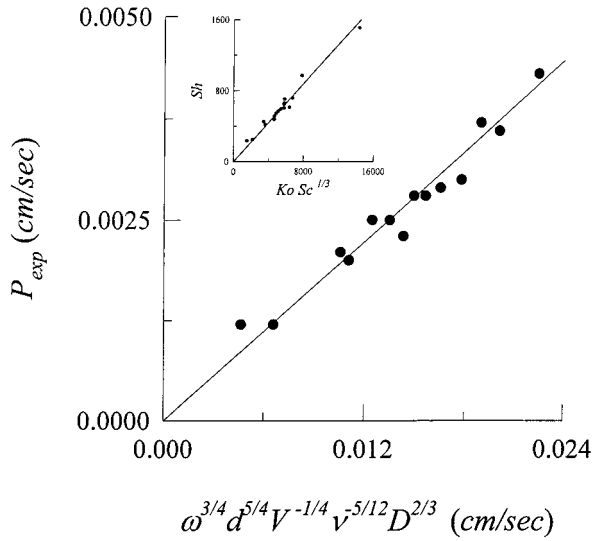


**Figure 4**—Generation of master curve for evaporation under turbulent flow conditions and liquid-side transport control. The *P* was correlated with the product ($\omega^{3/4}d^{5/4}V^{-1/4}\nu^{-5/12}D^{2/3}$), $r^2 = 0.95$. The data were obtained from evaporation of MC at $T \geq 25$ °C (liquid-side transport control, see Figure 5). The proportionality constant, *a*, was 0.18. Insert: The master curve in dimensionless form: *Sh* is correlated with $Ko \cdot Sc^{1/3}$ ($r^2 = 0.97$) for the same data set.

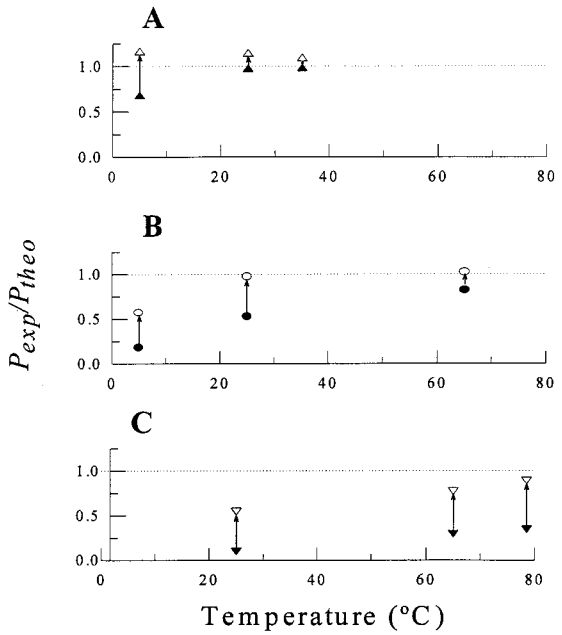


**Figure 5**—The influence of the gas-phase resistance to solvent evaporation. The gas-phase boundary layer was either unaltered (closed symbols) or disrupted by light $N_2$(g) flow over the air–water surface (open symbols). The ratio of experimental permeability to that calculated from the master curve obtained in Figure 4 (i.e., $P_{exp}/P_{theo}$) was determined for (A) methylene chloride, (B) ethyl acetate, and (C) acetonitrile.

included in the master curve (Figure 4; i.e., MC at 25 and 35 °C), the increase was not substantial (<15%). This result indicated that the gas phase had negligible resistance to the transport of MC under these conditions, which is consistent with the assumptions used to arrive at eq 16. In contrast, as *T* was decreased to 5 °C, the presence of $N_2$ (g) raised the value of $P_{exp}$ near the value expected by liquid-side control as determined with eq 16. This large difference in $P_{exp}$ induced by $N_2$ flow justifies the exclusion of the 5 °C data in Figure 4.

EA and ACN were selected for evaluation because their Henry's law constants, *H*, favor gas-phase control relative to MC. Because $P_L$ or $P_G$ should not strongly depend on the type of solvent, *H* was used as an indicator of the gas to obey liquid-side transport control at a given temperature according to eq 3. In Table 1, the relative trend of the values of *H* for various solvents at constant *T* is given. Because MC has a low bp (and a high saturated vapor pressure, $p^v$) and a low solubility in water ($C_s$), *H* ($\sim p^v/C_s$) must be a relatively high value. Because EA has a higher bp (therefore a lower $p^v$) and a higher $C_s$ than MC, it must have a lower *H* (i.e., *H* = medium). Finally, because ACN has an equivalent bp to EA but is completely miscible with water, the *H* for ACN must be even lower (i.e., *H* = low). Therefore, it is expected that the trend favoring liquid-side transport control is MC > EA > ACN.

**Table 1—Properties of Organic Solvents Examined for Evaporation**[a]

| organic solvent | bp (°C)[b] | $p^v$ | $C_s$ (w/w) | H ($\sim p^v/C_s$) | observed transport control at 25 °C[f] |
|---|---|---|---|---|---|
| MC | 40 | high | 2.0%[c] | high | liquid |
| EA | 77 | med | 6.92%[d] | med | mixed (gas/liq) |
| ACN | 82 | med | miscible[d] | low[e] | gas |

[a] Abbreviations: bp normal boiling point; $p^v$, saturated vapor pressure; $C_s$, aqueous solubility; *H*, Henry's law constant. [b] Values were taken from ref 15. [c] Values at 25 °C were taken from ref 16. [d] Values at 25 °C were taken from ref 15. [e] $H \sim p^v/C_s$ only applicable to EA and MC. ACN is completely miscible with $H_2O$ resulting in a very low *H*. [f] See Table 2.

As shown in Figures 5B and 5C, as *T* was increased, $P_{exp,\ w/o\ N_2(g)}$ for EA and ACN approached both the $P_{exp,\ w/N_2\ (g)}$ and the $P_{theo}$, as was the trend for MC just described. Also as expected, the resistance in the gas phase was steadily more difficult to overcome as *H* was decreased (following the trend MC < EA < ACN), indicating the gas-phase resistance increases as *H* decreases. At 25 °C the transport control was in the liquid phase for MC, in both liquid/gas phases for EA, and in the gas phase for ACN (Table 1). These data are consistent with (1) the validity of the correlation in eq 16 to predict *P* under liquid-side transport control conditions, and (2) the presence of significant gas-phase resistance when *H* becomes too low.

**Independence of $\delta_D$ on *T***—The theoretical boundary layer thickness in the liquid phase varied from ~30 to 170 $\mu$m, as shown in Table 2 (which also summarizes the evaporation data). The range of $\delta_D$ values determined from theory are consistent with typical values quoted from the literature.[7] A particularly notable trend was the independence of $\delta_D$ on *T*. In Table 2, for protocol #1−5, $\delta_D \sim 45\ \mu$m for a temperature range of 5−40 °C. This theoretical result was also confirmed experimentally as indicated by the equivalence of $P_{exp,w/N_2\ gas}$ and $P_{theo}$ for this data set.[25]

**Determination of Concentration-Dependent Permeability Coefficient**—To make practical use of the evaporation treatment described here, the evaporation was related to the formulation of the microspheres; that is, microsphere hardening kinetics. To illustrate this relationship, the permeability coefficient in the concentration-dependent regime was acquired under the same conditions used during the encapsulation (vide infra). To obtain a reliable permeability coefficient $P(C)$ for the calculation, multiple pure evaporation experiments were performed (three of them from pure water and one of them from 0.3% PVA aqueous solution[17]). After fitting each group of data with a 4th-order polynomial (see eq 11), the data were normalized by plotting ln *C* versus ($t - a_0$), as shown in Figure 6A. This normalization was necessary because MC is so volatile that it is very difficult to start at an exact

**Table 2—Summary of Evaporation of Organic Solvents from the Aqueous Hardening Bath**

| protocol # | solvent | $T$ (K) | $\nu \times 10^{-3}$ (cm$^2$/s) | $D \times 10^{-5}$ (cm$^2$/s) | $V$ (cm$^3$) | $d$ (cm) | $\omega$ (rpm) | $A_{exp}$ (cm$^2$) | $P_{exp} \times 10^{-3}$ (cm/s) | $P_{theo} \times 10^{-3}$ (cm/s)[a] | $\delta_D$ (=$D/P_{theo}$) ($\mu$m) | transport control[b] |
|---|---|---|---|---|---|---|---|---|---|---|---|---|
| 1 | MC | 313 | 6.75 | 1.84 | 150 | 3 | 600 | 35.5 | 4.32 | 4.15 | 44.3 | liq |
| 2[c] | MC | 308 | 7.42 | 1.65 | 150 | 3 | 600 | 35.5 | 3.63 (4.04) | 3.71 | 44.5 | liq |
| 3 | MC | 303 | 8.21 | 1.47 | 150 | 3 | 600 | 35.5 | 2.96 | 3.29 | 44.6 | liq |
| 4[c] | MC | 298 | 9.14 | 1.29 | 150 | 3 | 600 | 35.5 | 2.80 (3.29) | 2.90 | 44.7 | liq |
| 5[c] | MC | 278 | 15.0 | 0.73 | 150 | 3 | 600 | 35.5 | 1.08 (1.86) | 1.60 | 45.7 | gas/liq |
| 6 | MC | 303 | 8.21 | 1.47 | 150 | 3 | 900 | 44.5 | 4.75 | 4.46 | 32.9 | liq |
| 3 | MC | 303 | 8.21 | 1.47 | 150 | 3 | 600 | 35.5 | 2.96 | 3.29 | 44.6 | liq |
| 7 | MC | 303 | 8.21 | 1.47 | 150 | 3 | 450 | 33.7 | 2.43 | 2.65 | 55.3 | liq |
| 8 | MC | 303 | 8.21 | 1.47 | 150 | 3 | 300 | 29.9 | 2.09 | 1.96 | 75.0 | liq |
| 9 | MC | 303 | 8.21 | 1.47 | 150 | 3 | 100 | 27.4 | 1.15 | 0.86 | 170.8 | liq |
| 3 | MC | 303 | 8.21 | 1.47 | 150 | 3 | 600 | 35.5 | 2.96 | 3.29 | 44.6 | liq |
| 10 | MC | 303 | 8.21 | 1.47 | 200 | 3 | 600 | 35.5 | 2.90 | 3.06 | 47.9 | liq |
| 11 | MC | 303 | 8.21 | 1.47 | 250 | 3 | 600 | 35.5 | 2.78 | 2.90 | 50.6 | liq |
| 12 | MC | 303 | 8.21 | 1.47 | 300 | 3 | 600 | 35.5 | 2.67 | 2.77 | 53.0 | liq |
| 13 | MC | 303 | 8.21 | 1.47 | 450 | 3 | 600 | 35.5 | 2.52 | 2.66 | 55.1 | liq |
| 14[d] | MC | 303 | 8.21 | 1.47 | 1000 | 3 | 600 | 224.7 | 2.04 | 2.05 | 71.6 | liq |
| 15[d] | MC | 303 | 8.21 | 1.47 | 1000 | 3 | 300 | 217.7 | 1.22 | 1.22 | 120.4 | liq |
| 16[d] | MC | 303 | 8.21 | 1.47 | 1000 | 5 | 300 | 224.2 | 2.52 | 2.31 | 63.6 | liq |
| 17[d] | MC | 303 | 8.21 | 1.47 | 1000 | 7 | 300 | 246.4 | 3.69 | 3.51 | 41.8 | liq |
| 18[c] | EA | 338 | 4.52 | 2.35 | 150 | 3 | 600 | 35.5 | 4.81 (5.99) | 5.78 | 40.7 | gas/liq |
| 19[c] | EA | 298 | 9.14 | 1.01 | 150 | 3 | 600 | 35.5 | 1.29 (2.57) | 2.45 | 41.1 | gas/liq |
| 20[c] | EA | 278 | 15.0 | 0.57 | 150 | 3 | 600 | 35.5 | 0.25 (0.78) | 1.36 | 41.9 | gas |
| 21[c] | ACN | 352 | 3.80 | 4.23 | 150 | 3 | 600 | 35.5 | 3.33 (8.42) | 9.19 | 46.1 | gas/liq |
| 22[c] | ACN | 338 | 4.52 | 3.40 | 150 | 3 | 600 | 35.5 | 2.28 (5.84) | 7.38 | 46.0 | gas/liq |
| 23[c] | ACN | 298 | 9.14 | 1.46 | 150 | 3 | 600 | 35.5 | 0.35 (0.84) | 3.14 | 46.5 | gas |

[a] $P_{theo} \equiv a\,\omega^{3/4} d^{5/4} V^{-1/4} \nu^{-5/12} D^{2/3}$ (where $a$ is the regression constant), according to linear regression of master curve in Figure 4. [b] Transport governed by liquid-side (liq), gas-side (gas), or a combination (gas/liq). [c] Blowing of $N_2$(g) over the air/liquid surface was also performed for this protocol; value of $P_{exp}$ for blowing experiment is given in parentheses. [d] The large glass vessel instead of the jacketed beaker was used to perform the evaporation study.

concentration at a precise designated time. Also shown in the figure, the second-, third-, fourth-, and sixth-order polynomial fit (according to eq 23) for the same group of data all interpolated the data extremely well. To select the optional $p_n(\ln C)$, the slope of each polynomial was compared with the slope of the data as $C$ approaches $C_s$, as shown in Figure 6B. Among $n = 2$, 3, 4, and 6, the optional fit according to this criterion was between $n = 3$ an 4, so $p_3(\ln C)$ was selected for future use.

**Predicting Microsphere Hardening Kinetics**—To test the ability to predict the hardening profile, a drug soluble in MC, triamcinolone acetonide, was encapsulated in PLGA microspheres under standard conditions of encapsulation. These data are shown in Figure 7. The normalized MC concentration in the continuous phase (i.e., $C/C_s$) became essentially saturated ($C^* \sim 1$) for the first 40 min, and then declined sharply until negligible solvent remained by 200 min. The normalized MC concentration in the dispersed phase (i.e., $C_{DP}/C_{DP}^0$) declined exponentially over this time interval until the particles were dry.

Also shown in Figure 7 is the 6$^{th}$-order interpolating function of $C(t)$, $q_6(t)$. From $q_6(t)$ and $p_3'(\ln q_6(t))$, the hardening profile $M_H(t)$ was predicted and displayed in Figure 8. The theoretical $M_H$ matched very closely with the experimental value determined from the $C_{DP}$ versus $t$ data shown in Figure 7. Thus, both the concentration-dependent $P(C)$ determined without encapsulation and the experimental procedure to detect $C$ and $C_{DP}$ have been validated.

**Distribution of Organic Solvent during Encapsulation**—The distribution of MC during encapsulation of triamcinolone acetonide is depicted in Figure 9. Note again, over the first 40 min, the concentration of MC in the continuous phase was nearly saturated. It is important to note that hardening still occurred over this time interval, despite this elevated bath concentration, at a rate very similar to the evaporation rate.[18] Thus, the hardening rate during this interval was limited by evaporation. After this period, the hardening rate declined and the MC amount in the continuous phase began to fall below saturation. The

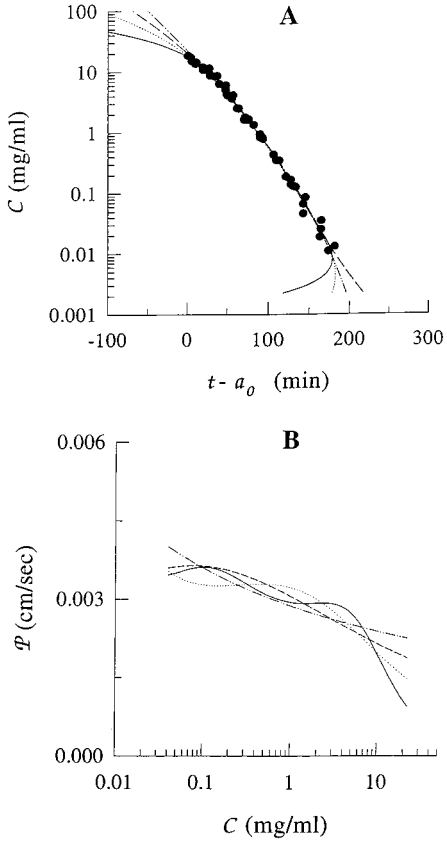


**Figure 6**—(A) Determination of the interpolating $n^{th}$ order polynomial function to describe the permeability coefficient. The 2$^{nd}$ (–•••–), 3$^{rd}$ (– –), 4$^{th}$ (••••), and 6$^{th}$ (—)-order polynomial functions, $p_n(\ln C)$, were fitted according to eq 21 for the normalized evaporation data ($n = 4$). (B) The dependence of $P$ on $C$ (log-scale), as determined from the derivative of the $n^{th}$ order polynomial interpolating functions with respect to ln $C$ according to eq 25.

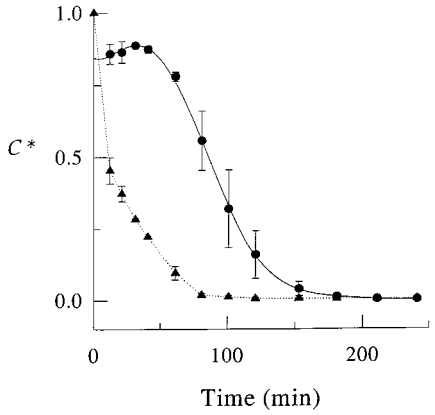


**Figure 7**—The concentration decline of MC during microencapsulation of triamcinolone acetonide by the solvent evaporation method. The concentration in dispersed (▲) and continuous phases (●) were normalized by the initial MC concentration in the polymer $C_{DP}^0$ (i.e., $C^* = C_{DP}/C_{DP}^0$) and by the solubility of MC in 0.3% PVA aqueous solution (i.e., $C^* = C/C_s$), respectively. The plotted data are mean ± SD ($n = 2$). (—) is a sixth-order polynomial fit, $q_6(t)$, and (·····) connects data points.

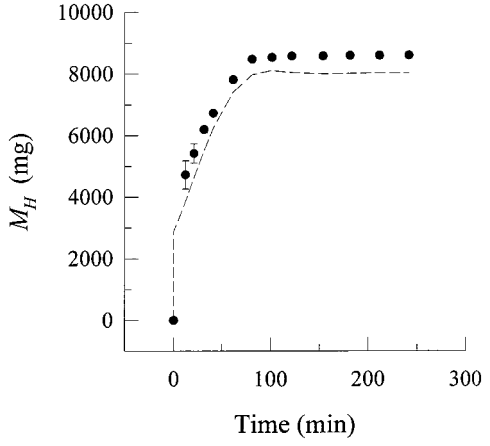


**Figure 8**—Predicting the hardening profile during microencapsulation of triamcinolone acetonide from $q_6(t)$ and $p_3'(\ln q_6(t))$. The microsphere hardening profile was measured (●) and predicted (– – –). The plotted data are mean ± SD ($n = 2$).

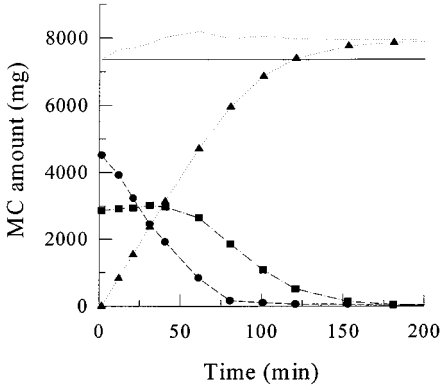


**Figure 9**—The distribution of MC during microencapsulation of triamcinolone acetonide. The mass of MC was determined in the dispersed phase (●), the continuous phase (■), and the surroundings (evaporated) (▲) during the hardening of the microspheres. The overall mass recovered from the calculation (·····) showed good agreement with the initial MC in the hardening bath (—).

sum of MC mass from experimentally determined $C$, $C_{DP}$, and the theoretical loss of MC to surroundings ($\int R_E dt$) accounted for 104−110% of the mass during the entire encapsulation experiment.

For completeness, microspheres thus formed were observed to be spherical under the microscope and had a size distribution of 44 ± 18 (mean ± SD, $n = 100$) by light microscopic size determination. The triamcinolone acetonide loading was 3.9 ± 0.2% (mean ± SD, $n = 6$) as determined by HPLC after dissolution of the polymer in acetonitrile.[19] Control studies also revealed that the controlled-release function of these microspheres was intact; that is, release was slow and continuous for >30 days.

## Discussion

**Identification of Process Variables that Control Solvent Evaporation**—The most efficient method to change the evaporation rate was to adjust $\omega$, $d$, or $T$. The effect of $V$ was very weak (−1/4 power dependence). As indicated by the similarity of $P_{exp}$ and $P_{theo}$ in Table 2 (usually <15% error when under liquid phase transport control), the relationship in eq 16 is well validated. This result suggests the potential to accurately affect the hardening rate of microspheres by manipulating the continuous phase concentration, $C$, during encapsulation. Specific applications of eq 16 will be pursued in a future paper.

**Rate-Limiting Step for Mass Transport during Evaporation**—As shown in the *Theoretical Section*, the resistance to mass transport in an evaporation system originates from two major sources: the diffusion layers in the liquid and gas phases. Because these two resistance are in series, if one resistance is much greater than the second, the greater of the two will largely determine the overall resistance. If the unstirred layer is relatively thin in the gas phase (or resistance is very small) compared with the liquid phase, the overall mass transport barrier will reside in the liquid phase. Under these conditions, the $P$ of the evaporation system can be predicted by eq 16 with reasonable accuracy (Table 2). If the resistance in the gas phase is not too large to be reduced effectively by $N_2$ gas flow, the $P$ may still be predicted by eq 16 with acceptable accuracy, as evidenced by the data for MC at 5 °C and for EA at 25 °C (Figure 5).

The analysis in Figure 5 confirms the hypothesis that the Henry's law constant and temperature are the predominant indicators of whether a specific organic solvent evaporates according to gas- or liquid-side transport control. Dissolved gases, such as $O_2$, with extremely high values of $H$ will always be liquid-side transport limited,[20] and solvents such as ACN that are highly soluble in water with lower vapor pressure (i.e., low $H$) will be expected to be gas-side transport limited. A particularly notable result was that MC at room temperature is liquid-side transport limited, whereas EA, a frequently used alternative in encapsulation, has a significant resistance in the gas phase at this temperature. This result suggests that blowing $N_2$ (g), as performed here and elsewhere,[21] may be appropriate for the use of EA at room temperature.

**Physical Description of Solvent Evaporation from the Hardening Bath**—It was demonstrated that under the most common encapsulation conditions (i.e., MC evaporation at room temperature in turbulent flow), the evaporation largely falls under liquid-phase transport control. Two important concepts underlie the mass transport in the liquid-phase boundary layer. The first concept is turbulence. The nature of the turbulence induced by the impeller controls the size and speed of the smallest eddies that approach the evaporating surface. The eddy of size $\sim\delta_K$ is formed by an energy cascade, which begins with large eddies that are unstable and break up into steadily smaller liquid "packages" of chaotic movement. At the scale where local $Re \sim 1$, the fluid elements lose their kinetic energy to thermal energy. Because $\delta_K$ is only dependent on the

kinematic viscosity and the total energy per unit mass (or volume) of fluid according to the assumption of isotropic turbulence, the evaporation rate is somewhat independent of bath geometry after correction for the surface area at the air/water interface. There is, however, a small dependence of $P$ on bath volume because more fluid means more fluid mass available to dissipate the turbulent energy. This dependence as well as the dependence of $P$ on $d^{5/4}$, have obvious scaling implications.

The second concept is the velocity distribution in the viscous sublayer and how it is affected by the approaching eddy to the free air/water surface. The velocity distribution affects the relationship between the diffusion layer thickness and viscous sublayer thickness (by either $Sc^{-1/2}$ or $Sc^{-1/3}$). Because organic solvents are surface active,[22] we must have the equivalent of the 'dirty' surface case, which is similar hydrodynamically to the liquid/solid interface. This hypothesis was confirmed by the validity of eq 16, which would not have been so if a "clean" surface was assumed. The parabolic velocity distribution in the sublayer leads to the well-known variation of $\delta_D$ with $Sc^{-1/3}$.[23]

**The Role of Solvent Evaporation on Microsphere Hardening during Microencapsulation**—Because the microsphere hardening profile was successfully predicted with $P(C)$ and $C$ without directly measuring $C_{DP}$, it is theoretically possible in the future to continuously monitor the microsphere hardening kinetics by simply measuring $C$ during encapsulation provided that the $P(C)$ is known. It is also reasonable to envision on-line systems to monitor the continuous-phase organic solvent concentration during encapsulation. Because the microsphere hardening kinetics may directly affect the final microsphere quality, the monitored results could potentially be used as quality control criteria for microsphere production.

It is important to note, however, that it is expected that the evaporation will only play a dominant role in the microsphere hardening kinetics if two conditions are satisfied: (1) the extraction capacity of the continuous phase has been saturated; and (2) the diffusion rate of organic solvents from the dispersed phase (DP) to the continuous phase (CP) is fast compared with the solvent evaporation kinetics. The first condition is determined by the organic solvent solubility in continuous aqueous phase and the initial DP/CP volume ratio. The second prerequisite, however, will be much more complicated and influenced by several factors, including the initial organic solvent extraction rate, polymer MW and concentration, and temperature of encapsulation.[24] All these factors are directly related to the microsphere hardening conditions and remain to be investigated in the future.

In closing, the mechanism of evaporation during solvent evaporation encapsulation processes has been elucidated, confirmed experimentally, and used to predict microsphere hardening kinetics. These results have potential use for formulation, design of encapsulation apparatus, and scaling-up of microsphere production.

## Nomenclature

$A$ = surface area of air−water interface, $cm^2$
$C$ = organic solvent concentration in the continuous phase of the bath, mg/mL
$C_0$ = initial organic solvent concentration in the continuous phase of the bath, mg/mL
$C_{DP}$ = MC content in the dispersed polymer phase, mg/mg PLGA
$C_{DP}^0$ = initial MC content in the dispersed polymer phase, mg/mg PLGA
$C_S$ = solubility of organic solvent in the continuous phase of the bath, mg/mL
$C_T$ = MC content in the entire aqueous dispersion, mg/mL
$C^*$ = normalized MC content in continuous phase ($C^* = C/C_s$) or in dispersed phase (DP; $C^* = C_{DP}/C_{DP}^0$), unitless
$D$ = diffusion coefficient of the organic solvent in the continuous phase of the bath, $cm^2/s$
$d$ = impeller diameter, cm
$H$ = Henry's law constant, atm·mL/mg
$j_s$ = organic solvent flux at the air/liquid interface, mg/($cm^2$·s)
$Ko$ = corrected Kolmogorov number, $d/(\delta_K \cdot N_p^{1/4})$, unitless
$M_B$ = molecular weight of aqueous solvent in the bath, g/mol
$M_H$ = cumulative mass removed from microspheres, mg
$M_P$ = mass of PLGA in the dispersed aqueous system, mg
$N_P$ = power number, unitless
$P$ = overall permeability coefficient, cm/s
$P_G$ = permeability coefficient in the gas phase, mg/(atm·$cm^2$·s)
$P_L$ = permeability coefficient in the liquid phase, cm/s
$p_n$ = $n^{th}$-order polynomial interpolating function for $t$ versus ln $C$ during evaporation, min
$\dot{Q}$ = rate of energy loss from the impeller to the fluid, g·$cm^2/s^3$
$q_m$ = $m$th-order polynomial interpolating function for $C$ vs $t$ during encapsulation, mg/mL
$R_E$ = organic solvent evaporation rate, mg/min
$R_H$ = overall rate of organic solvent removal from microspheres (i.e., hardening rate), mg/min
$Re$ = impeller Reynolds number, $\omega d^2/\nu$, unitless
$Re^*$ = local Reynolds number, $u_e\delta_e/\nu$, unitless
$Sc$ = Schmidt number, $\nu/D$, unitless
$Sh$ = Sherwood number, $Pd/D$, unitless
$T$ = temperature, K
$t$ = time, min or s
$u_e$ = velocity of the eddies approaching air−water interface, $\mu$m/s
$V$ = volume of fluid in the hardening tank, mL
$V_A$ = molar volume of organic solvent at its boiling temperature, $cm^3$/mol
$\delta_e$ = length scale of the eddies approaching air−water interface, $\mu$m
$\delta_D$ = diffusion sublayer thickness, $\mu$m
$\delta_K$ = Kolmogorov length scale, $\mu$m
$\delta_V$ = viscous sublayer thickness, $\mu$m
$\epsilon$ = energy dissipation rate per unit mass fluid, $cm^2/s^3$
$\nu$ = kinematic viscosity, $cm^2/s$
$\eta_B$ = viscosity of aqueous solution in hardening bath, cp
$\omega$ = rotational speed of overhead stirrer, rev/s or rpm
$\Phi$ = association factor (for prediction of $D$), unitless
$\Psi$ = ratio of the volume of the continuous phase to the volume of the entire aqueous dispersion, unitless
$\rho$ = density of aqueous solution in hardening bath, mg/mL

## References and Notes


1. Thies, C. Formation of Degradable Drug-Loaded Microparticles by In−Liquid Drying Processes. In *Microcapsules and Nanoparticles in Medicine and Pharmacy*; Donbrow, M., Ed.; CRC: Ann Arbor, MI, 1991; pp 47−71.
2. Arshady, R. Preparation of Biodegradable Microspheres and Microcapsules: 2. Polyactides and Related Polyesters. *J. Controlled Release* **1991**, *17*, 1−22.
3. Crotts, G.; Park, T. G. Preparation of Porous and Nonporous Biodegradable Polymeric Hollow Microspheres. *J. Controlled Release* **1995**, *35*, 91−105.
4. Li, W. I.; Anderson, K. M.; Mehta, R. C.; Deluca, P. P. Prediction of Solvent Removal Profile and Effect on Properties for Peptide-Loaded PLGA Microspheres Prepared by Solvent Extraction/Evaporation Method. *J. Controlled Release* **1995**, *37*, 199−214.
5. Jeyanthi, R., Thanoo, B. C.; Metha, R. C.; Deluca, P. P. Effect of Solvent Removal Technique on the Matrix Characteristics

of Polylactide/Glycolide Microspheres for Peptide Delivery. *J. Controlled Release* **1996**, *38*, 235−244.
6. Oldshire, J. Y. *Fluid Mixing Technology*; Chemical Engineering: New York, 1983; pp 43−71.
7. Cussler, E. L. *Diffusion-Mass Transfer in Fluid Systems*; Cambridge University: New York, 1984; pp 215−248, 172−193.
8. Hunt, J. C. R. Turbulence Structure and Turbulent Diffusion Near Gas−Liquid Interfaces. In *Gas Transfer at Water Surfaces*; Brutsaert, W.; Jirka, G. H., Eds.; D. Reidel Publishing: Dordrecht, Holland, 1984; pp 67−82.
9. Blevins, R. D. Dimensional Analysis. In *Applied Fluid Dynamics Handbook*; Blevins, R. D., Ed.; Van Nostrand Reinhod: New York, 1984; pp 8−18.
10. Perry, R. H.; Green, D. W.; Maloney J. O. *Perry's Chemical Engineers' Handbook*, 6th ed.; McGraw-Hill: New York, 1984; pp 19-(5−14), 3-(75−77).
11. Gillett, P. *Calculus and Analytic Geometry*; D. C. Heath and Company: Lexington, MA, 1981; pp 290−294.
12. Reid, R. C.; Prausnitz, J. M.; Poling B. E. *The Properties of Gases and Liquids*, 4th ed.; Sun, B., Fleck, G. H., Eds.; Mcgraw-Hill: New York, 1987; pp 52−54, 388−485, 577−626.
13. To perform the prediction of $M_H$ with reasonable accuracy, the hardening rate must be of a similar magnitude or greater than the evaporation rate. If $R_H \ll R_E$, then the common problem of taking the difference of two very close large experimental values is encountered.
14. Boyce, W. E.; Diprima, R. C. *Elementary Differential Equations*, 3rd ed.; John Wiley & Sons: New York, 1977; pp 358−361.
15. Smallwood, I. M. *Handbook of Organic Solvent Properties*; John Wiley & Sons: New York, 1996; pp 37, 227, 289.
16. Horvath, A. L. *Halogenated Hydrocarbons Solubility-Miscibility with Water*; Marcel Dekker: New York, 1982; pp 658−660.
17. The presence of PVA had no influence on the experiment described in Figure 6A so the data with and without PVA were combined for the determination of the interpolating function, $p_n(t)$.
18. It was unexpected to observe such a high hardening rate as $C \rightarrow C_s$ because the chemical potential of MC in the DP cannot be greater than the chemical potential in the CP at $C = C_s$. Therefore, the hardening must proceed with a very small chemical driving force (i.e., difference between the chemical potential in the DP and the chemical potential in the continuous phase).
19. Zhou, T. H.; Lewis, H.; Foster, R. E.; Schwendeman, S. P. Development of a Multiple-Drug Delivery Implant for Intraocular Management of Proliferative Vitreoretinopathy. *J. Controlled Release* **1998**, *55*, 281−295.
20. Sherwood, T. K.; Pigford R. L.; Wilke C. R. *Mass Transfer*; Clark, B. J.; Maisel, J. W., Eds.; McGraw-Hill Book Company: New York, 1975; pp 101−196.
21. Cleland, J. L.; Jones, A. J. S. Stable Formulations of Recombinant Human Growth Hormone and Interferon-$\gamma$ for Microencapsulation in Biodegradable Microspheres. *Pharm. Res.* **1996**, *13(10)*, 1464−1475.
22. Sluzky, V. Insulin Stability and Aggregation in Agitated Aqueous Solutions. Ph.D. Thesis, Massachusetts Institute of Technology, Cambridge, MA, 1992.
23. Levich, V. G. *Physicochemical Hydrodynamics*; Amundson, N. R., Ed.; Prentice-Hall: Englewood Cliffs, NJ, 1962; pp 139−183.
24. Li, Wen-I. Mechanism and mathematical modeling of microsphere formation. Ph.D. Thesis, University of Kentucky, Lexington, KY, 1994.
25. The fascinating independence of $\delta_D$ on $T$ stems from the negligible temperature dependence of the product, $\nu^{5/12}D^{1/3}$, in eq 17.

## Acknowledgments

This work was supported in part by NIH DE 12183 and an OSU Comprehensive Cancer Center support grant (NIH P30 CA 16058). Support to Juan Wang was also provided by an OSU multiple year university fellowship.

JS980169Z